03 Mar 2023

Hyperspectral Reflectance for Determination of Steel Rebar Corrosion and Cl− Concentration

Pengfei Ma

Liang Fan

Genda Chen
Missouri University of Science and Technology, gchen@mst.edu

Recommended Citation

P. Ma et al., "Hyperspectral Reflectance for Determination of Steel Rebar Corrosion and Cl− Concentration," *Construction and Building Materials*, vol. 368, article no. 130506, Elsevier, Mar 2023. The definitive version is available at https://doi.org/10.1016/j.conbuildmat.2023.130506

Construction and Building Materials 368 (2023) 130506

Contents lists available at ScienceDirect

Construction and Building Materials

journal homepage: www.elsevier.com/locate/conbuildmat

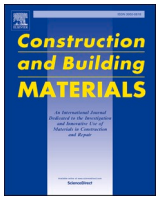

Hyperspectral reflectance for determination of steel rebar corrosion and Cl^- concentration

Pengfei Ma [a], Liang Fan [b,c,*], Genda Chen [a]

[a] Department of Civil, Architectural and Environmental Engineering, Missouri University of Science and Technology, Rolla, MO 65401, United States
[b] Key Laboratory of Marine Environmental Corrosion and Bio-fouling, Institute of Oceanology, Chinese Academy of Sciences, Qingdao 266071, China
[c] Institute of Marine Corrosion Protection, Guangxi Academy of Sciences, Nanning 530007, China

ARTICLE INFO

Keywords:
Steel corrosion
Hyperspectral imaging
Reflectance intensity
Short-wave infrared spectroscopy
Open circuit potential
Cl^- concentration

ABSTRACT

In this study, a new method is proposed to determine chloride ion (Cl^-) concentration and steel rebar corrosion from hyperspectral spectroscopy. Three groups of mortar cubes with water-to-cement (w/c) ratios of 0.5, 0.6, and 0.7 were subjected to rapid corrosion testing in 3.5 wt% NaCl solution to accelerate the transport of chloride ions. Embedded along the centerline of each mortar cube was a steel rebar that corroded when the Cl^- accumulation around it exceeded a critical/threshold concentration. Open circuit potential was measured to characterize the corrosion possibility of steel rebar. Mortar surfaces were scanned with a hyperspectral camera in the infrared range (1000 nm – 2400 nm), and the reflectance intensity at 2258 nm wavelength was extracted to characterize Friedel's salt. The possibility of steel corrosion was experimentally shown to increase with the characteristic reflectance intensity that in turn decreases linearly with the diffusion depth at a given corrosion state. For each type of mortar cubes with a constant w/c ratio, the characteristic reflectance intensity linearly increases with the Cl^- content up to 0.8 wt%. Therefore, the corrosion status of steel rebar and Cl^- concentration can be predicted based on the combined information from the reflectance intensity on the mortar surface and the relation between reflectance and total chloride content.

1. Introduction

Corrosion of steel rebar has long been viewed as the primary cause that leads to the degradation of reinforced concrete (RC) structures and induces durability problems especially on bridges [1]. In 2013, the annual direct cost induced by steel corrosion was estimated to be $13.6 billion for highway bridges, and indirect cost due to traffic delay could be more than 10 times [2]. In the highly alkaline environment of concrete, a dense passive film is generated on the surface of rebar to prevent it from corrosion. However, the ingress of Cl^- can gradually cause acidification in the vicinity of rebar and make the passive film unstable [3–4]. When the accumulated Cl^- content reaches a critical threshold, the passive film will be destroyed and corrosion initiates on the rebar surface. In the literature, the critical threshold value mainly ranges from 0.2% to 0.7% and can even go up to 2.5% by the weight of cement for the outdoor concrete [5]. Corrosion products physically occupy higher volume than steel, and their expansion causes cracks or even spalling in concrete covers [6–8]. Corrosion also reduces the cross-sectional area of steel rebar and thus bearing capacity of the structural component [9–10]. Therefore, it is imperative to rapidly identify potential corrosion regions in embedded steel rebar for in-time treatment before they lead to any structural deficiency.

Chloride ion concentration in RC structures needs to be closely monitored to prevent the potential detrimental corrosion induced risks. There are widely used destructive ways to measure Cl^- content in concrete, including pulverization and titration. To avoid destructive tests, several types of embeddable sensors have been developed to monitor Cl^- concentration. For example, an embeddable Ag/AgCl electrode was used to linearly relate the measured potential variation to Cl^-concentration when it exceeded 62 ppm [11]. However, embedment of the electrode requires space inside the concrete and thus causes discontinuity in RC components. Additionally, this method to quantify Cl^- concentration is highly affected by temperature, humidity, and alkalinity [12]. Similarly, a calcium-alginate sol–gel (a fluorescent patch) based spectrometer can be used to determine Cl^- concentration from the intensity of reflective light as light absorbance is altered when Cl^- is in contact with the fluorescent patch. Nevertheless, this sensor faces photodegradation and leaching-out issues in a high alkaline concrete environment [13]. A

* Corresponding author.
E-mail address: fanl@qdio.ac.cn (L. Fan).

https://doi.org/10.1016/j.conbuildmat.2023.130506
Received 8 January 2022; Received in revised form 20 January 2023; Accepted 22 January 2023
Available online 28 January 2023

capacitive technique was also applied to assess Cl^- concentration by analyzing permittivity in presence of chlorides, and the complex permittivity change was quantitatively correlated with Cl^- content at the frequency of 10 MHz. Unfavorably, other concrete ingredients such as aggregates will determinatively influence the capacitance, thus causing the drift of frequency [14–15].

Hyperspectral imaging has been introduced as a noninvasive technique to characterize the composition of materials in civil engineering [16]. Unlike ordinary RGB images that show objects in visible bands (VIs: 400–700 nm), hyperspectral images provide a continuous electromagnetic spectrum over wavelengths ranging from VIs to near infrared (NIR: 800–1200 nm) and far to short-wave infrared (SWIR: 1200–2500 nm), which can be decomposed to a massive number of bands [17]. Hyperspectral imaging is a three-dimensional data cube as illustrated in Fig. 1. Given a pixel, hyperspectral imaging yields a continuous reflectance curve as a function of wavelength [18]. The shape of the reflectance curve at bands, known as spectral signature [19], is governed by the presence of different chemical stretch combinations and thus enables the spectroscopic analysis of chemical compositions on the scanned surface.

Spectroscopy technique has been used to detect Cl^- content in RC structures. A laser induced breakdown spectroscopy was reported to create plasma radiation for elemental analysis on concrete surfaces when the Cl^- concentration exceeds 0.2 wt% [20]. A small-scale NIR spectroscopy system - an integration of imagery Fourier spectroscopy was developed to scan concrete surfaces [21]. The results show that both Cl^- concentration distribution and cracks on the concrete surface can be effectively detected. In the spectroscopic view, Cl^- content in the concrete is described and confirmed to be highly correlated with the reflectance at 2258 nm wavelength in the SWIR region, which indicates the presence of Friedel's salt [22–24]. As Cl^- penetrates through concrete and accumulates around the surface of embedded rebar to a threshold value, corrosion happens on the steel surface. If the distribution of Cl^- concentration across the concrete cover is obtained, chloride concentration on the steel rebar surface can be determined to evaluate the possibility of corrosion in steel rebar.

In this study, electrical current was impressed in each mortar cube to accelerate Cl^- penetration and steel corrosion. After corrosion states of steel rebar were determined from the measured open circuit potential (OCP), spectral curves of the selected points were extracted to indicate the chloride content gradient of mortar cubes along the depth. A rapid chloride test (RCT) was then conducted to determine the Cl^- concentration which was correlated with the reflectance intensity at 2258 nm wavelength corresponding to Friedel's salt. This correlation can be applied to predict the Cl^- concentration near a steel rebar and its corrosion state based on spectroscopic analysis.

2. Method

2.1. Sample preparation and experiment setup

A total of 27 cubic specimens (76 mm × 76 mm × 76 mm) were cast and divided into three groups with nine specimens in each group with a w/c ratio of 0.5, 0.6, or 0.7. These w/c ratios, as shown in Table 1, correspond to three mortar mixture proportions by weight of 0.182/0.364/1.0, 0.194/0.324/1.0, and 0.204/0.292/1.0 for water, Type I/II Portland cement, and Missouri river sand, respectively. The physical properties of Missouri river sand and the ordinary Portland cement are listed in Table 2 and Table 3, respectively. Embedded along the centerline of each cubic specimen is a steel rebar with a diameter of 12.7 mm and a length of 110 mm. One end of the steel rebar was soldered to a copper wire. Both ends of the rebar were then covered with marine epoxy to avoid corrosion during tests.

Fig. 2 illustrates the setup of a rapid diffusion test after 28 days of mortar curing. A PVC tube (Φ60mm) with a height of 40 mm was attached to the top surface of each cubic specimen and filled with 3.5 wt % NaCl solution. A stainless-steel rectangular plate (3 cm × 2.4 cm) was placed in the PVC tank and immersed in the NaCl solution. The bottom of the mortar specimen rested on a wet sponge and then a thin steel sheet to construct a circuit to propel the movement of chloride ions. Both the sponge and steel sheet were immersed in water. The steel sheet and the stainless-steel plate were respectively connected to the positive and negative poles of a power supply. A stable current of 3 mA was applied to accelerate the transport process of Cl^- through the mortar and this process lasted 3 h per day [25].

2.2. Electrochemical measurement of steel rebar

All samples were measured with open circuit potential (OCP) test to determine the corrosion state of steel rebar. Fig. 3 illustrates a standard test setup to determine the OCP at different stages with the steel rebar and a saturated calomel electrode (SCE, Gamry instrument, USA) as working and reference electrodes, respectively [26].

The electrodes were connected to a Potentiostat (Interface 1000, Gamry instrument, USA) during electrochemical experiments. Prior to

Table 1
Mixture composition of mortar samples by weight (kg/m^3).

Water/cement ratio	0.5	0.6	0.7
Water	270	287	302
Type I/II Portland cement	540	480	432
Missouri river sand	1482	1482	1482

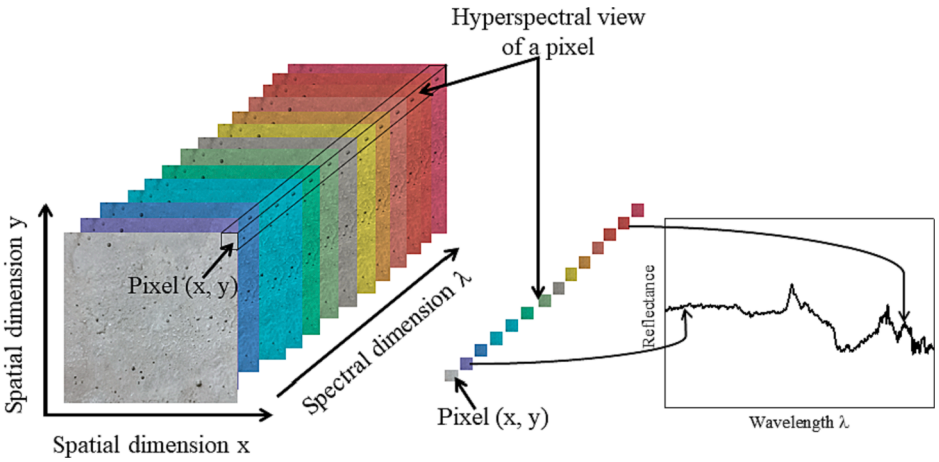

Fig. 1. Illustration of hyperspectral data cube.

Table 2
Properties of Missouri river sand.

Properties	Maximum particle size	Gravity	Fineness modulus
Missouri river sand	4.75 mm	2.64 g/cm^3	2.71

Table 3
Mass percentage of oxides in Type I/II Portland cement (%).

SiO_2	CaO	Al_2O_3	Fe_2O_3	MgO	SO_3	Loss of ignition
19.8	64.2	4.5	3.2	2.7	3.4	2.6

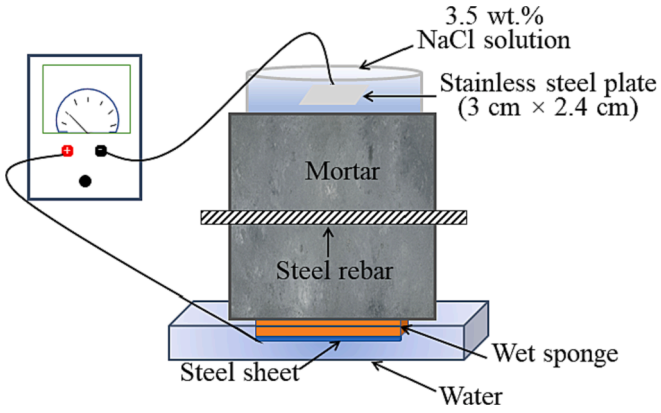

Fig. 2. Chloride ion diffusion test setup.

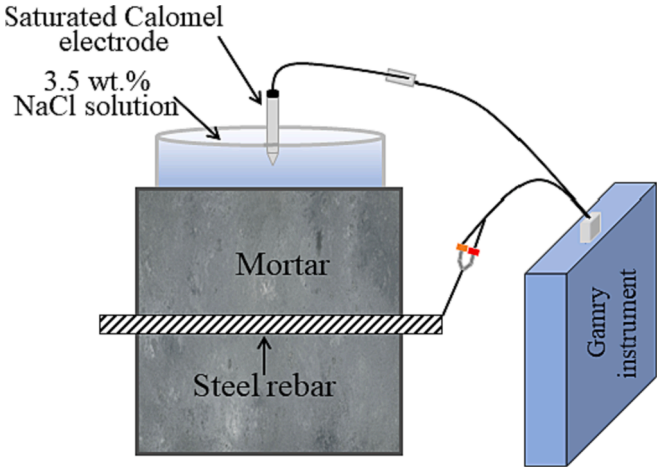

Fig. 3. Experimental setup for OCP measurement.

the test, samples were allowed a 3-hour break after the rapid chloride diffusion test for depolarization. When stabilized in 30 min, the OCP of each sample was taken.

OCP denotes the resting potential measured between reference and working electrode to define whether the electrochemical system stabilized. The potential of the metal is featured by the balance of the anodic and cathodic reactions. At OCP point, the net electron flow is zero [27]. As specified in [7], OCP, denoted as E_{ocp}, can be used to predict the corrosion status of steel rebar as shown in Table 4. The OCP values are periodically measured until they reach −126 mV/SCE, −276 mV/SCE and −400 mV/SCE, which represent three thresholds for rebar corrosion at different possibility states.

Table 4
E_{ocp} versus the corresponding corrosion status.

E_{ocp}(Saturated Calomel electrode)	> −126 mV	< −276 mV	<-400 mV
Probability of corrosion	10%	90%	severe

2.3. Hyperspectral scanning of mortar cubes

Fig. 4(a) displays the test setup for hyperspectral scanning of a sample with a co-aligned dual-sensor camera (Hyperspectral sensors, Headwall Photonics Inc, USA). This camera enables spectral measurement over wavelengths ranging from 400 nm to 2400 nm. The camera was fixed on the rack and set at 1.2 m standoff distance from the sample to be scanned. To provide proper illumination on the sample, a Quartz Tungsten-Halogen (QTH) lamp was set at 0.5 m distance with an incident angle of 45° as indicated in Fig. 4(a). The camera was connected to a laptop with Hyperspec-III software for both the setup of camera parameters and the collection of scanning data. Samples were placed on a conveyor that can run at a speed of up to 1 m/s. In this study, the conveyor was operated at 0.05 m/s to avoid image distortion. The frame period and exposure time of the camera were adjusted properly to guarantee a 60% saturated light intensity detection. Before scanning samples, the camera was calibrated by collecting dark and white references directly in the SpectralView software. The dark and white

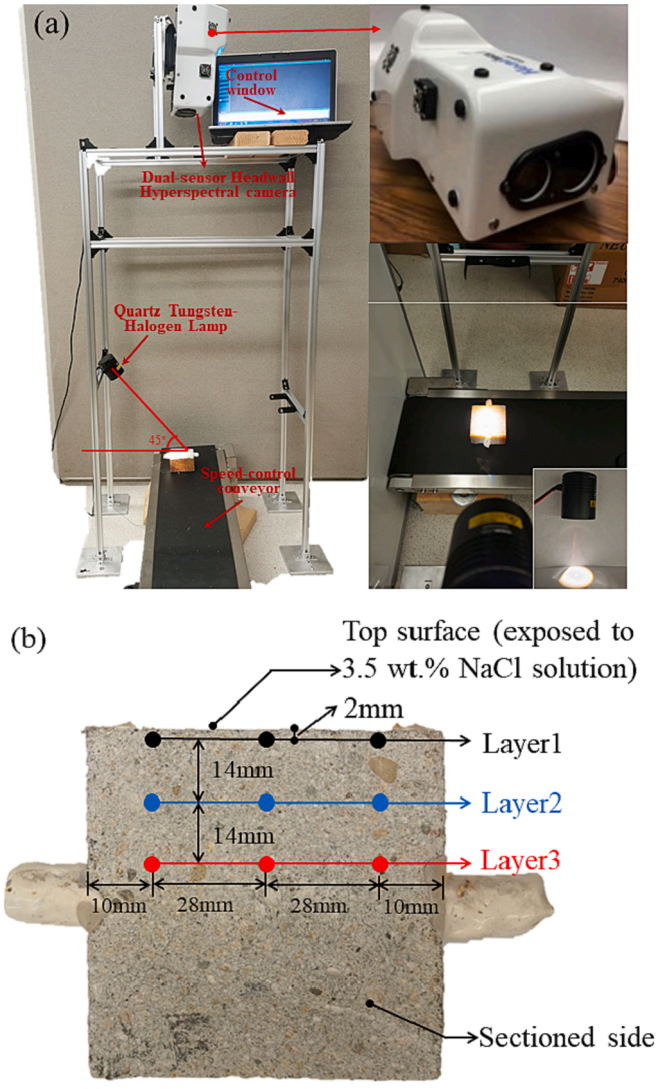

Fig. 4. Demonstration of (a) hyperspectral scanning of a specimen, and (b) selected points for hyperspectral imaging and rapid Cl^- testing.

references were used to normalize the reflectance of mortar specimens [28] as follows.

$$\text{Reflectance} = \frac{Raw - Dark}{White - Dark} \times White\ Reference\ Calibration \quad (1)$$

After the E_{ocp} of steel rebar reached each of the OCP threshold levels as specified in Table 4, each sample was cut open vertically at the pre-determined section by an electrical saw without water in case that water may dissolve the chloride containing salts on the sectioned surface. The pre-determined section was at approximately 2 mm away from the steel rebar for hyperspectral scanning. On each scanned face, three layers to cover various depths with three points of interest in each layer, as seen in Fig. 4(b), were investigated. The spectral curves at the three points in the same layer were averaged to obtain the representative spectral curve for the layer, which is more robust than an individual spectral curve. For each point of interest, it is derived from the integration of the 16 pixels (4 pixels × 4 pixels) in the vicinity. The spectral curve of each point was recorded using SpectralView software.

2.4. Baseline and bias correction of spectral signature for spectroscopy analysis

The reflectance spectra were collected for specific chemical analysis on the surface of mortar samples following the spectroscopy method. In addition to the chemical component, however, the reflectance changes with the spectral fluctuation of white and black references, the surface roughness and color variation of different mortar samples (or different measurements of the same sample due to corrosion over time), and illumination differences during testing of different samples. To eliminate the influence of the above factors, spectral curves collected from mortar samples are subjected to the baseline correction (likely caused by reference spectral fluctuation) for each curve and the bias correction (likely caused by mortar variation and illumination difference) between curves.

Fig. 5 presents the averaged spectral curves at three points of layer 1 under three corrosion scenarios. In general, the main composition of mortar paste does not yield spectral features between 1000 nm and 1700 nm except at the valley around 1410 nm [29]. For example, Fig. 5 indicates that the spectral curves are relatively flat from 1000 nm to 1300 nm and the reflectance value at 1300 nm is close to that at 1700 nm. Baseline correction for each spectral curve was thus conducted by removing a linear spectral drift between 1302 nm and 2400 nm, which is determined by the reflectance values near 1300 nm and 1700 nm as illustrated in Fig. 5(a). Specifically, the reflectance values on the solid curve in Fig. 5 (a) are 0.217 at 1302 nm and 0.224 at 1702 nm, having a subtle difference of 0.007 in reflectance. The linear spectral drift is expressed as

$$\sigma = (w - 1702) \times \frac{(0.224 - 0.217)}{(1702 - 1302)} = 1.75 \times 10^{-5} \times (\mathrm{w} - 1702) \quad (2)$$

and then was subtracted from the solid spectral curve in Fig. 5(a). Here, w is the wavelength at a specific band.

After baseline correction has been done for all spectral curves, bias correction is conducted by shifting the spectral curves upward or downward to make their reflectance values at 1302 nm equal. 1302 nm is selected because the main components of the cement paste do not yield reflectance features here [29]. For example, the solid spectral curve in Fig. 5(a) was used as a benchmark with a reflectance of 0.217 at 1302 nm and the dashed and dotted curves with a reflectance of 0.195 and 0.191, respectively, were shifted upward so that their reflectance at 1302 nm is equal to 0.217. After the baseline and bias corrections, the reflectance values under three different corrosion scenarios in Fig. 5(b) are nearly overlapped in the region of 1000 nm to 1700 nm, which is referred to as nonactive bands as far as the specific chemical analysis in the range of 1700 nm to 2400 nm is concerned. Thus, spectroscopic comparison can be conducted regardless of different corrosion states or

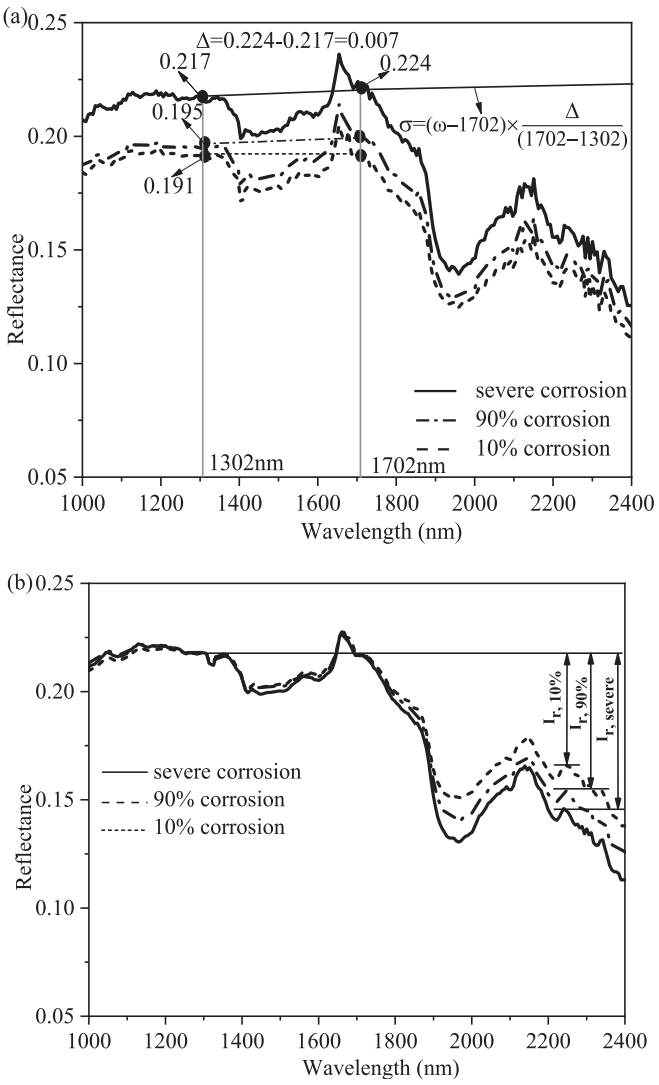

Fig. 5. Spectral curves at layer 1 on a mortar sample (w/c = 0.5) under three corrosion states (a) before baseline and bias correction, and (b) after baseline and bias correction.

mortar groups.

To represent the reflectance response of a certain chemical component from the spectral curve, reflectance intensity (I_r) is introduced and defined as the difference between the reflectance (I_{act}) of an active band of the target component and that (I_{1302}) of the nonactive band at 1302 nm. The reflectance intensity can be expressed as

$$I_r = I_{act} - I_{1302} \quad (3)$$

For instance, Friedel's salt yields a reflectance peak at 2258 nm and thus the reflectance intensity of Friedel's salt is $I_r = I_{2258} - I_{1302}$ as shown in Fig. 5(b).

2.5. Determination of Cl^- concentration by the RCT method

The Cl^- in the vicinity of steel rebar surface is accumulated to a critical threshold value to break down the passive film formed on the steel surface, thus initiating corrosion. Measurement of Cl^- content is carried out after steel rebar reached the corresponding corrosion status specified in Table 4. The commonly used method in measuring the chloride content is to extract the chloride ions with acid solution as specified in ASTM C1152 [30]. In the acid extraction method, all chloride ions in mortar powder, both water and acid soluble, are released

into the solution due to acidization. In this study, RCT kit (Rapid Chloride Test, Germann Instrument GI, USA), is adopted to measure the concentration of chloride ions. In practice, mortar powder was collected with a drill bit from the points in each layer as shown in Fig. 4(b). For each layer, the total amount of mortar powder from the three sampling points was 1.5 g. Mortar powder samples were then added to the RCT vials and shaken for 5 min to make them fully blended with acid solution. All RCT vials were remained for 24 h to allow the full release of the chloride ions into solution. The chloride concentration measurement was then carried out with the sensitive chloride ion electrode. The electrode chamber was firstly saturated with wetting agent and calibrated in advance by 0.005%, 0.020%, 0.050% and 0.500% chloride calibration liquids. Afterwards, the RCT electrode was immersed in the sample solutions to take the readings. The corresponding chloride concentration was obtained by interpolating the reading in the calibration curve which is usually a straight line [31].

3. Results and discussion

3.1. Evolution of E_{ocp}

As specified, E_{ocp} reflects the corrosion states of steel rebar with thresholds of −126 mV/SCE, −276 mV/SCE, and −400 mV/SCE indicating 10% and 90% probability of corrosion, and severe corrosion, respectively [6]. Fig. 6 shows the evolution of E_{ocp} of the steel rebar embedded in three groups of mortar samples. E_{ocp} kept above −126 mV at the beginning as the passive film on the surface of steel rebar still provided protection against corrosion. Then, E_{ocp} started to decrease moderately to −276 mV, indicating a high possibility of the occurrence of rebar corrosion due to the chloride ions ingress. An abrupt decrease below −400 mV was observed afterwards, so the protective passive film on rebar was damaged because of the accumulation of chloride ions and indicated the occurrence of corrosion. To achieve the same corrosion possibility on steel rebar, the mortar group with a lower w/c ratio (0.5) generally takes longer time than the other mortar groups (w/c = 0.6 or 0.7) because of the denser mortar matrix to reduce the chloride ion transport rate [5].

3.2. Spectroscopic analysis of chemical compound on the sectioned mortar cube surface

Fig. 7 displays a spectral curve of reflectance vs wavelength in NIR (1000 to 2400 nm) range for a region of interest on the scanned mortar surface. From the perspective of spectroscopic analysis, peaks and dips

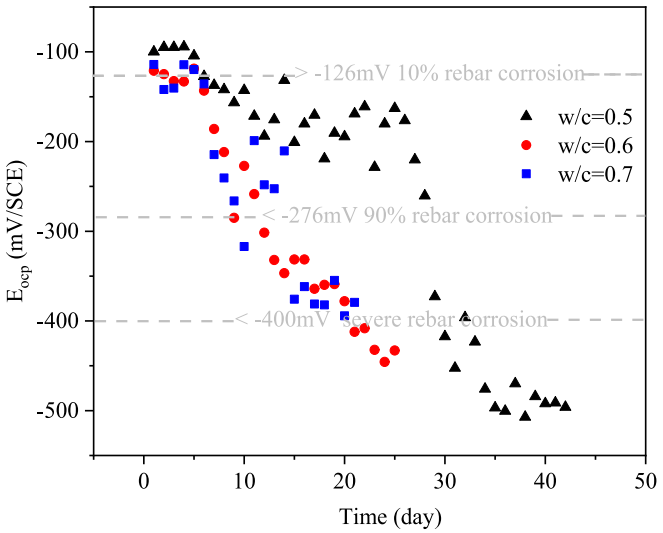

Fig. 6. Evolution of E_{ocp} for mortar samples of different w/c ratios.

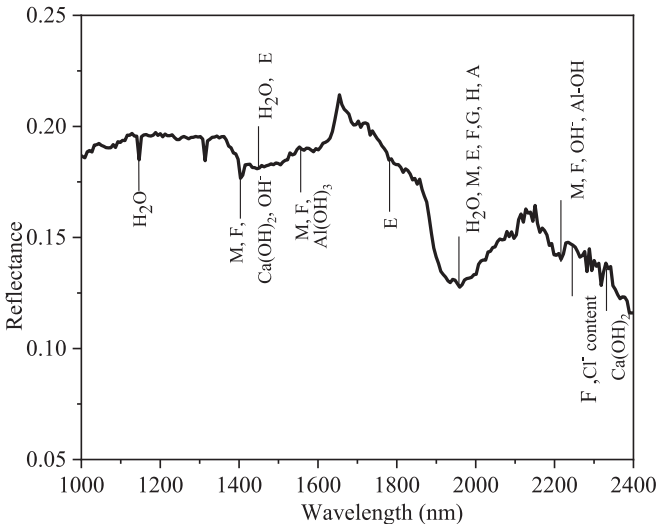

Fig. 7. A typical spectrum extracted from the mortar cut surface.

are attributed to the reflectance and absorbance of light by the specific molecular or chemical bond of atoms. As shown in Fig. 7, many calcium hydrates and chlorides related products yield features on the curve. Some feature may indicate more than one component such as H_2O, $Ca(OH)_2$, and ettringite at wavelength of 1410 nm. On the other hand, one component may have more than one feature such as $Ca(OH)_2$ at wavelength of 1385 nm, 1410 nm and 2360 nm. Table 5 lists the chemical compounds that can be detected with hyperspectral technology. For spectroscopic analysis, such features can be utilized to evaluate the presence of some substances, and the intensity at a wavelength is related to the corresponding concentration [22]. Friedel's salt, the dominant chloride product, is featured at a small bump at 2258 nm [29]. In this study, the Friedel's salt is employed to detect Cl^- concentration and predict corrosion states of steel rebar afterwards.

Fig. 8 summarizes the reflectance spectra in NIR (1000 to 2400 nm) range after baseline and bias correction at the selected points on the sectioned faces of representative samples with w/c ratios of 0.5, 0.6 and 0.7. Each spectral curve is obtained by averaging the spectra values of three points at the same layer as illustrated in Fig. 4 (b). The spectrum remains flat between 1000 nm and 1400 nm as the compounds on the mortar sample surface do not yield special features in this region.

Table 5
The characteristic wavelengths for identifying mortar components.

Component	Wavelength (nm)	Reference
H_2O	1135	[19]
H_2O	1380	[29,33,34]
Monosulphate(M)	1385	[29]
Friedel's salt (F)	1385	[29]
$Ca(OH)_2$, OH^-	1385	[29]
H_2O	1410	[32–34]
$Ca(OH)_2$	1410	[29]
Ettringite (E)	1410	[29]
$CaSO_4$	1750	[32–33]
Ettringite (E)	1760	[29]
Gypsum (G), Hemihydrates (H)	1780	[32]
H_2O	1950	[29]
Gypsum (G), Anhydrite (A), Hemihydrates (H)	1950	[32]
Si–OH	2173	[32]
Ettringite (E), Gypsum (G)	2173	[32]
Al-OH, OH^-	2226	[32]
Friedel's salt (F)	2258	[19,29,33–34]
$Ca(OH)_2$	2360	[22]
Ettringite (E)	2470	[35]

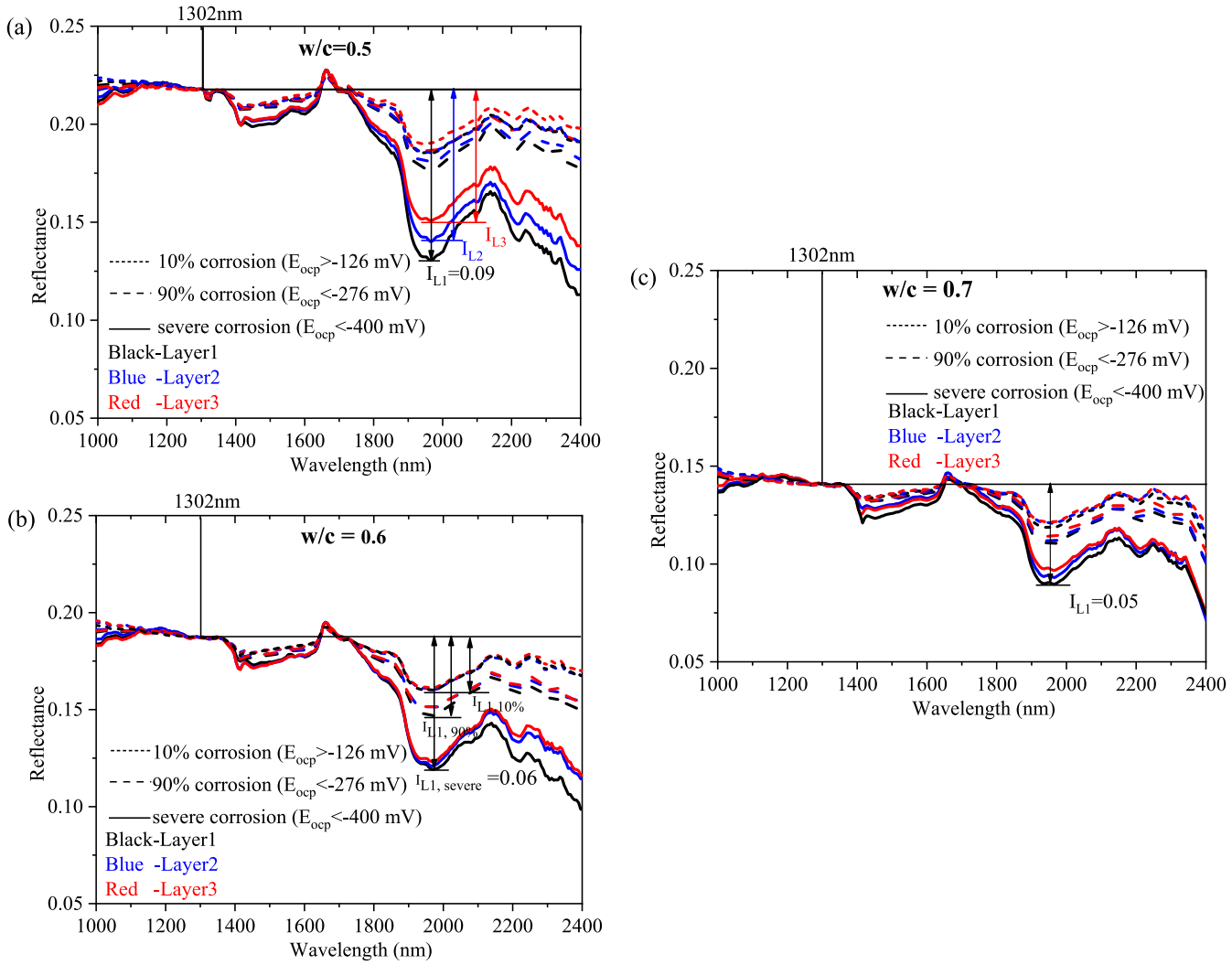

Fig. 8. Averaged reflectance spectra of three selected points after correction at each layer on the cross-section of representative samples with a w/c ratio of (a) 0.5, (b) 0.6, and (c) 0.7.

Followed in the range of 1400 nm to 1700 nm is a wide reflectance valley induced by the moisture and various hydrates. Remarkable differences can be observed between 1700 nm and 2400 nm within a mortar group mainly owing to the abundance of the chemical compounds such as water, Friedel's salt ($3CaO \bullet Al_2O_3 \bullet CaCl_2 \bullet 10H_2O$), ettringite ($3CaO \bullet Al_2O_3 \bullet 3CaSO_4 \bullet 32H_2O$), and calcium hydroxide as indicated in Table 5. The variation between curves ascribes to the w/c ratios of mortar and duration of the chloride diffusion test as longer duration facilitates both physical change and chemical reaction in terms of chloride products and other related mortar compounds mentioned in Fig. 7. For spectroscopic comparison, the reflectance intensity (I_r) decreases from layer 1 (top surface) to layer 3 at the same corrosion state. I_{L3}, I_{L2} and I_{L1} are in an ascending order in all three corrosion states as shown in Fig. 8(a). For steel rebar with higher possibility of corrosion, major mortar constituents yield a higher reflectance feature within the range from 1700 nm and 2400 nm. $I_{L1,\ 10\%}$, $I_{L1,\ 90\%}$ and $I_{L1,\ severe}$ at layer1 are in an increasing order as illustrated in Fig. 8(b), which is applicable to cases of layer 2 and layer 3. It is also noted that higher reflectance intensity within 1700 nm and 2400 nm for mortar groups with lower w/c ratios. For instance, the I_{L1} at the same corrosion state decreases from 0.09 to 0.05 with an increase of w/c ratio from 0.5 to 0.7.

3.3. Relation between corrosion status and reflectance intensity at 2258 nm

Fig. 8 demonstrates that the reflectance intensity has a positive correlation with the possibility of rebar corrosion occurrence which is characterized by E_{oc}. To illustrate the chloride content induces rebar corrosion, the small spike at wavelength 2258 nm, corresponding to Friedel's salts, is used to reflect the concentration of chloride ions in the mortar [30]. Fig. 9 shows the reflectance intensity (I_r) at 2258 nm (Friedel's salts featured) from layer 1 to layer 3 and its correlation with the corrosion probability of rebar embedded in three mortar groups. Triangle, round, and square shapes represent the specimens with w/c ratios of 0.5, 0.6, and 0.7, respectively. The shapes are filled with black, blue and red colors, representing the data measured from layer 1, layer 2 to layer 3, respectively. Each data point in the figure represents the average value of three measure points in the same layer as shown in Fig. 4(b).

As depicted in Fig. 9, the overall reflectance intensity has an increasing trend when w/c ratios decrease from 0.7 to 0.5. Considering E_{ocp}, lower E_{ocp} higher corrosion possibility) are correspondingly indicated by higher reflectance intensity, I_r. For example, for the black dash line with triangle marks, reflectance intensity at layer1 increase from 0.013 to 0.020 and to 0.041 when the E_{ocp} decrease from −126 mV to −276 mV and to −400 mV. Lower E_{ocp} requires more accumulation of

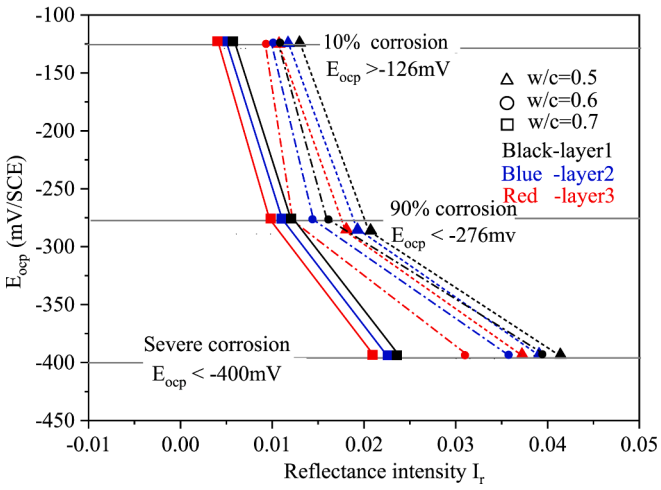

Fig. 9. The relations between reflectance intensity and E_{ocp} for all three groups of mortar samples.

chloride ions to corrode the steel rebar, and thus higher concentration of Friedel's salts yield larger reflectance intensity at 2258 nm. In addition, it can be seen that the reflectance intensity of three layers (black, blue and red) from mortar surface (layer 1) to rebar interface (layer 3) is strictly in a downward order regardless of the corrosion stages or w/c ratios of mortar. It is also observed that reflectance intensity at layer 3 on section faces of mortar cubes with different w/c ratios also varies. The lower w/c ratio corresponds to a higher reflectance intensity. The I_r at 2258 nm near rebar (layer3) are 0.037, 0.030 and 0.021 respectively for mortar samples with w/c ratio of 0.5, 0.6 and 0.7 considering severe corrosion stage ($E_{ocp} < -400$ mV).

The reflectance intensity has an indictive prediction of the possibility of rebar corrosion occurrence which is represented by E_{ocp}. It can be observed from Fig. 9 that reflectance intensity in rebar vicinity ranging from 0.018 to 0.037 indicates there is a 90% or higher corrosion chance for steel rebar embedded in mortar samples with a w/c ratio of 0.5. Under the same corrosion probability circumstance, the reflectance intensity is above 0.011 and 0.0098 for mortar samples with w/c of 0.6 and 0.7, respectively. To predict the corrosion states of steel rebar from the reflectance intensity on the surface (layer1) of mortar sample, the reflectance intensity pattern from top (layer 1) to center (layer 3) is established as shown in Fig. 10. I_r at 2258 nm generally decreases linearly along the diffusion depth though the decrease rate varies between groups. According to the spectroscopy indication, there is a 90% possibility that rebar corrodes in the mortar with w/c of 0.5 if the I_r at 2258 nm on the top surface of mortar reaches 0.021, while this critical I_r drops to 0.015 and 0.011 for mortar cubes with a w/c ratio of 0.6 and 0.7, respectively.

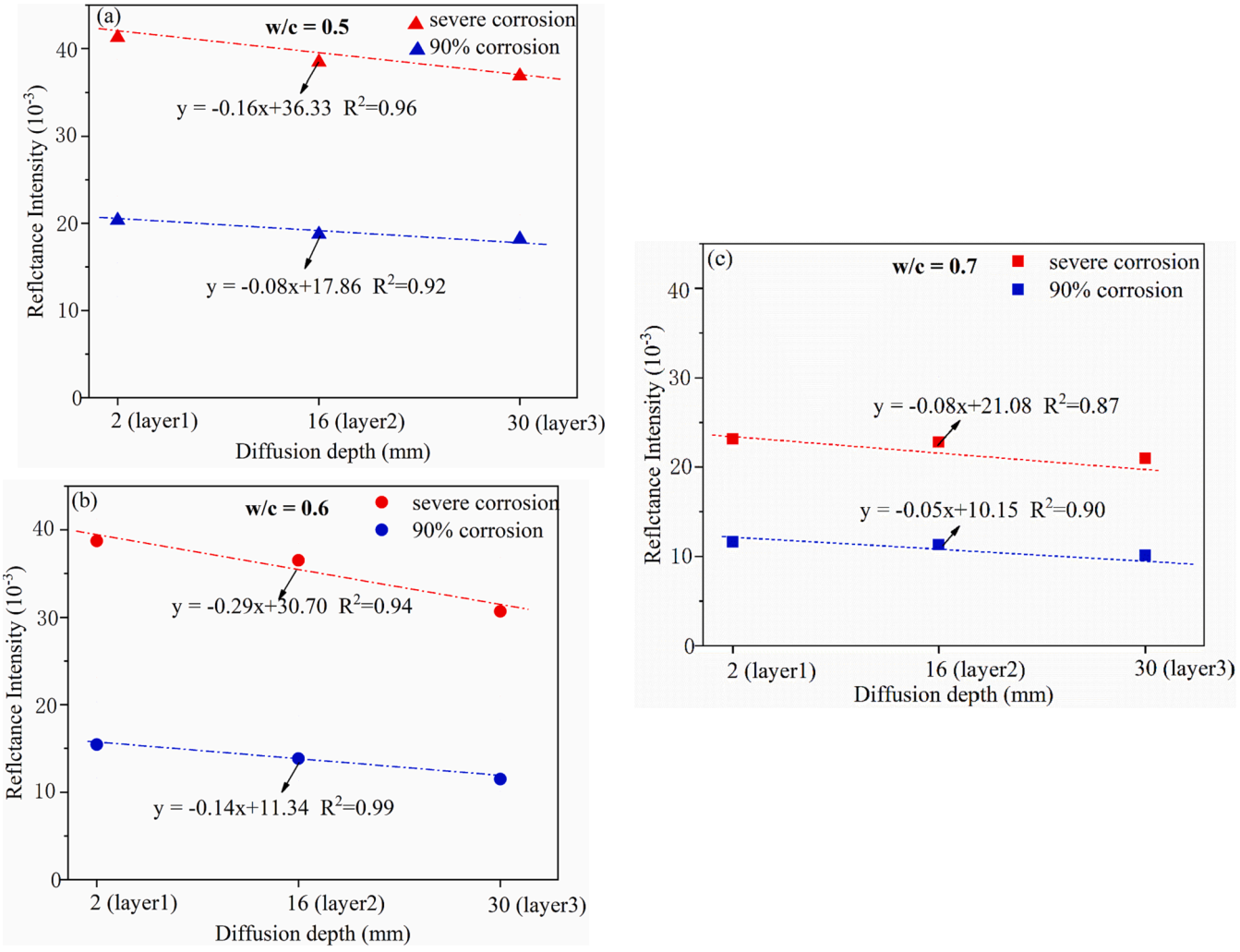

Fig. 10. The reflectance intensity trend along diffusion depth at cases of 90% corrosion probability and severe corrosion for samples with (a) w/c = 0.5, (b) w/c = 0.6, and (c) w/c = 0.7.

3.4. Relation between reflectance intensity I_r and chloride ion concentration

As the spectroscopic index can indirectly predict the chloride ion concentration and further demonstrate the possibility of rebar corrosion occurrence, the correspondence between I_r and actual chloride ion concentration on the sectioned faces for scenarios in Fig. 10 is established. Table 6 lists the measured chloride ion concentration in mortar powder collected from the points in each layer as specified in Fig. 4(b) when the E_{ocp} of the steel rebar is below −276 mV and −400 mV. As shown in Table 6, the measured chloride ion concentration drops from layer 1 (near the top surface) to layer 3 (near the steel rebar surface). For the same layer, the sample with a lower w/c ratio has higher Cl^- concentration. This is because the sample with a smaller w/c ratio has a denser microstructure, and more chlorides ions are bounded in the matrix [31]. As a result, more chloride ions are needed to transport to the surface of the steel rebar to disrupt the passive film and induce steel corrosion. The chloride ion concentration threshold near the steel rebar surface in case of severe corrosion ($E_{ocp} < -400mV$) varies from 0.58 wt % to 0.14 wt% when the w/c ratio of mortar increases from 0.5 to 0.7. Likewise, the chloride threshold is 0.16 wt%, 0.040 wt% and 0.025 wt% for 90 percent possibility of corrosion ($E_{ocp} < -276mV$).

Fig. 11 shows the measured total chloride ion content by weight of the cement versus the corresponding reflectance intensity at the same spots. Higher reflectance intensity corresponds to larger Cl^- concentration measured by the RCT. The reflectance intensity has a linear correlation with the total chloride content in all three groups of samples. The decreasing chloride concentration from the mortar surface to the vicinity of rebar proves the trace of chloride ions along the diffusion path. As the reflectance intensity is in linear relation with the chloride ion content along the penetration depth, with the known chloride concentration on the mortar surface, the corresponding chloride concentration near the steel rebar can be estimated according to Fig. 11. As a result, it is likely to predict the chloride content and thus predict the corrosion status of the rebar through reflectance intensity near the top surface of mortar that is exposed to the chloride solution.

4. Conclusions

This study investigates the feasibility of predicting steel rebar corrosion and chloride concentration through analyzing the reflectance intensity at 2258 nm on mortar surfaces. Open circuit potential was obtained to indicate the corrosion status of steel rebar, and chloride content was measured with rapid chloride tests. By correlating the reflectance intensity with the corrosion status of steel rebar and the chloride ion content of mortar sample powder, the following conclusions can be drawn:

1. The reflectance intensity at 2258 nm obtained from the spectroscopy analysis of mortar surfaces decreased with the mortar w/c ratio from 0.5 to 0.7. At a constant w/c, the higher the reflectance intensity, the lower the E_{ocp}.
2. The reflectance intensity along the chloride ion diffusion depth is linearly declining from mortar surface to the vicinity of rebar. It linearly increased with the chloride ion concentration.
3. The critical chloride concentration ranges from 0.16 wt% to 0.04 wt % and to 0.025 wt% to induce a 90% possibility of corrosion on steel rebar embedded in mortar cubes with w/c ratio of 0.5, 0.6 and 0.7, respectively. To predict the 90% possibility corrosion on rebar in mortar cubes, it is suggested that the reflectance intensity on the mortar top surface(layer1) surpasses 0.018, 0.011 and 0.0098 for the mortar cubes with w/c ratio of 0.5, 0.6 and 0.7, respectively.

The experimental results clearly show that the corrosion status of steel rebar and Cl^- concentration can be predicted from reflectance intensity near the top surface of mortar samples. Drone-based hyperspectral scanning is thus a promising technique to rapidly monitor corrosion induced deterioration on bridge decks. Future work will be directed to measure the reflectance intensity of concrete and mortar samples with a wide range of binder types to enlarge the reflectance dataset and re-establish the relationship between hyperspectral reflectance representing Friedel's salt and OCP values as well as the relation between hyperspectral reflectance and total chloride contents of mortar. To apply this technique in field cases, the effects of natural environmental factors such as carbonation on the hyperspectral reflectance acquired near the top surface of concrete/mortar will be tested as well for the accurate prediction of Cl^- induced steel rebar corrosion.

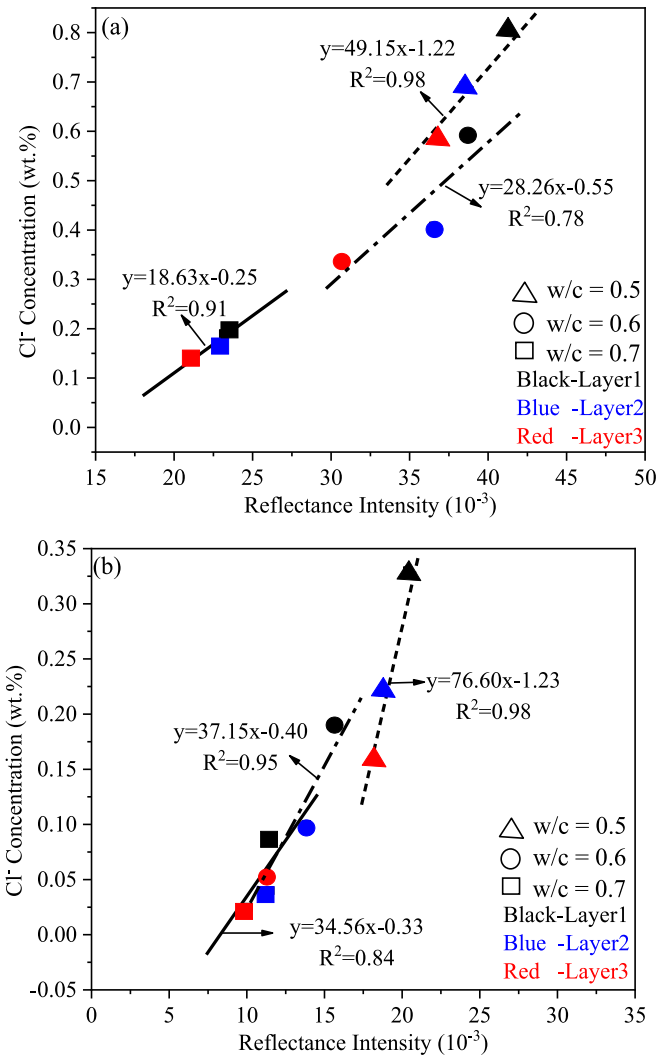

Fig. 11. Correlation between reflectance intensity and Cl^- concentration for samples when (a)E_{ocp} < -400 mV/SCE, (b)E_{ocp} < -276 mV/SCE.

Table 6
The measured chloride ion concentration of three groups of mortar samples in cases ofE_{ocp} < -276 mV/SCE andE_{ocp} < -400 mV/SCE (unit: wt.%).

E_{ocp}	<-276 mV (90% corrosion)			<-400 mV (severe corrosion)		
w/c ratio	0.5	0.6	0.7	0.5	0.6	0.7
Layer1	0.33	0.19	0.085	0.81	0.60	0.19
Layer2	0.22	0.10	0.050	0.69	0.41	0.17
Layer3	0.16	0.040	0.025	0.58	0.34	0.14

Funding

Financial support to complete this study was provided by the U.S. Department of Transportation, Office of the Assistant Secretary for Research and Technology (OST-R) under the Auspices of the INSPIRE University Transportation Center under Grant No. 69A3551747126 at Missouri University of Science and Technology.

CRediT authorship contribution statement

Pengfei Ma: Formal analysis, Methodology, Writing – original draft. **Liang Fan:** Conceptualization, Methodology, Formal analysis, Writing – review & editing, Supervision. **Genda Chen:** Writing – review & editing, Supervision.

Declaration of Competing Interest

The authors declare that they have no known competing financial interests or personal relationships that could have appeared to influence the work reported in this paper.

Data availability

Data will be made available on request.

References

[1] S. Baek, W. Xue, M.Q. Feng, S. Kwon, Nondestructive corrosion detection in RC through integrated heat induction and IR thermography, J. Nondestr. Eval. 31 (2) (2012) 181–190, https://doi.org/10.1007/s10921-012-0133-0.
[2] NACE (2013) Report on corrosion of highways and bridges in the US. NACE International. https://www.nace.org/resources/industries-nace-serves/highways-bridges.
[3] M.U. Khan, S. Ahmad, H.J. Al-Gahtani, Chloride-induced corrosion of steel in concrete: an overview on chloride diffusion and prediction of corrosion initiation time, Internat. J. Corr. 2017 (2017), https://doi.org/10.1155/2017/5819202.
[4] S. Mundra, M. Criado, S.A. Bernal, J.L. Provis, Chloride-induced corrosion of steel rebars in simulated pore solutions of alkali-activated concretes, Cem. Concr. Res. 100 (2017) 385–397, https://doi.org/10.1016/j.cemconres.2017.08.006.
[5] G.K. Glass, N.R. Buenfeld, The presentation of the chloride threshold level for corrosion of steel in concrete, Corros. Sci. 39 (5) (1997) 1001–1013, https://doi.org/10.1016/S0010-938X(97)00009-7.
[6] R.B. Figueira, Electrochemical sensors for monitoring the corrosion conditions of reinforced concrete structures: A review, Appl. Sci. 7 (11) (2017) 1157, https://doi.org/10.3390/app7111157.
[7] H. An, G. Meng, Y. Wang, J. Wang, B. Liu, F. Wang, Study on the chloride threshold and risk assessment of rebar corrosion in simulated concrete pore solutions under applied potential, Coatings 10 (5) (2020) 505, https://doi.org/10.3390/coatings10050505.
[8] L. Fan, W. Meng, L. Teng, K.H. Khayat, Effects of lightweight sand and steel fiber contents on the corrosion performance of steel rebar embedded in UHPC, Constr. Build. Mater. 238 (2020), 117709, https://doi.org/10.1016/j.conbuildmat.2019.117709.
[9] L. Fan, Y. Bao, W. Meng, G. Chen, In-situ monitoring of corrosion-induced expansion and mass loss of steel bar in steel fiber reinforced concrete using a distributed fiber optic sensor, Compos. B Eng. 165 (2019) 679–689, https://doi.org/10.1016/j.compositesb.2019.02.051.
[10] L. Fan, Y. Bao, G. Chen, Feasibility of distributed fiber optic sensor for corrosion monitoring of steel bars in reinforced concrete, Sensors 18 (11) (2018) 3722, https://doi.org/10.1016/j.compositesb.2019.02.051.
[11] S. Muralidharan, R. Vedalakshmi, V. Saraswathi, J. Joseph, N. Palaniswamy, Studies on the aspects of chloride ion determination in different types of concrete under macro-cell corrosion conditions, Build. Environ. 40 (9) (2005) 1275–1281, https://doi.org/10.1016/j.buildenv.2004.10.005.
[12] M. Torres-Luque, E. Bastidas-Arteaga, F. Schoefs, M. Sánchez-Silva, J.F. Osma, Non-destructive methods for measuring chloride ingress into concrete: State-of-the-art and future challenges, Constr. Build. Mater. 68 (2014) 68–81, https://doi.org/10.1016/j.conbuildmat.2014.06.009.
[13] M. Dhouib, D. Conciatori, L. Sorelli, Optical fiber chloride sensor for health monitoring of structures in cold regions, in: Cold Regions Engineering, American Society of Civil Engineers, Reston, VA, 2019, pp. 391–397, 10.1061/9780784482599.045.
[14] D.A. Koleva, J.H.W. De Wit, K. Van Breugel, L.P. Veleva, E. Van Westing, O. Copuroglu, A.L.A. Fraaij, Correlation of microstructure, electrical properties and electrochemical phenomena in reinforced mortar. Breakdown to multi-phase interface structures. Part II: Pore network, electrical properties and electrochemical response, Mater Charact 59 (6) (2008) 801–815, https://doi.org/10.1016/j.matchar.2007.06.016.
[15] G.S. Duffó, S.B. Farina, Development of an embeddable sensor to monitor the corrosion process of new and existing reinforced concrete structures, Constr. Build. Mater. 23 (8) (2009) 2746–2751, https://doi.org/10.1016/j.conbuildmat.2009.04.001.
[16] P.K. Mehta, P.JM. Monteiro, Concrete: Microstructure, Properties, and Materials, McGraw-Hill Education, 2014.
[17] C.I. Chang, Q. Du, Estimation of number of spectrally distinct signal sources in hyperspectral imagery, IEEE Trans. Geosci. Remote Sens. 42 (3) (2004) 608–619, https://doi.org/10.1109/TGRS.2003.819189.
[18] E. Sharifahmadian, S. Latifi, Advanced hyperspectral remote sensing for target detection, in: 2011 21st International Conference on Systems Engineering, IEEE, 2011, pp. 200–205, https://doi.org/10.1109/ICSEng.2011.43.
[19] R. Schneider dos Santos, S.B.A. Rolim, F. Hepp Pulgati, Application of visible and near infrared spectroscopy in non-destructive evaluation of cement materials, Int. J. Remote Sens. 36 (3) (2015) 917–938, https://doi.org/10.1080/01431161.2014.1001083.
[20] G. Wilsch, F. Weritz, D. Schaurich, H. Wiggenhauser, Determination of chloride content in concrete structures with laser-induced breakdown spectroscopy, Constr. Build. Mater. 19 (10) (2005) 724–730, https://doi.org/10.1016/j.conbuildmat.2005.06.001.
[21] Y. Sakakihara, Y. Kabeyama, H. Kanasaki, K. Hamada, S. Okazaki, K. Wada, I. Ishimaru, Chloride ion measurement system for RC structure by near-infrared spectroscopy, GEOMATE J. 19 (71) (2020) 48–54, https://doi.org/10.21660/2020.71.9258.
[22] M. Kohri, T. Ueda, H. Mizuguchi, Application of a near-infrared spectroscopic technique to estimate the chloride ion content in mortar deteriorated by chloride attack and carbonation, J. Adv. Concr. Technol. 8 (1) (2010) 15–25, https://doi.org/10.3151/jact.8.15.
[23] K.Y. Ann, H.W. Song, Chloride threshold level for corrosion of steel in concrete, Corros. Sci. 49 (11) (2007) 4113–4133, https://doi.org/10.1016/j.corsci.2007.05.007.
[24] V.S. Ban, B.L. Volodin, S. Dolgi, Determination of chloride ion concentration in concrete by means of near infra-red spectroscopy, in: Nondestructive Characterization for Composite Materials, Aerospace Engineering, Civil Infrastructure, and Homeland Security 2011, SPIE, 2011, pp. 634–640, 10.1117/12.880947.
[25] C. Boschmann Käthler, S.L. Poulsen, H.E. Sørensen, U.M. Angst, Investigations of accelerated methods for determination of chloride threshold values for reinforcement corrosion in concrete, Sustainable Resilient Infrastruct (2021) 1–12, https://doi.org/10.1080/23789689.2021.1905221.
[26] L. Ptacek, A. Strauss, B. Hinterstoisser, A. Zitek, Curing assessment of concrete with hyperspectral imaging, Materials 14 (14) (2021) 3848, https://doi.org/10.3390/ma14143848.
[27] C.Q. Ye, R.G. Hu, S.G. Dong, X.J. Zhang, R.Q. Hou, R.G. Du, C.J. Lin, J.S. Pan, EIS analysis on chloride-induced corrosion behavior of reinforcement steel in simulated carbonated concrete pore solutions, J. Electroanal. Chem. 688 (2013) 275–281, https://doi.org/10.1016/j.jelechem.2012.09.012.
[28] L. Fan, M. Fan, A. Alhaj, G. Chen, H. Ma, Hyperspectral imaging features for mortar classification and compressive strength assessment, Constr. Build. Mater. 251 (2020), 118935, https://doi.org/10.1016/j.conbuildmat.2020.118935.
[29] A. Watanabe, H. Furukawa, S. Miyamoto, H. Minagawa, Non-destructive chemical analysis of water and chlorine content in cement paste using near-infrared spectroscopy, Constr. Build. Mater. 196 (2019) 95–104, https://doi.org/10.1016/j.conbuildmat.2018.11.114.
[30] ASTM, C,, Standard Test Method For Acid-Soluble Chloride In Mortar And Concrete, ASTM International, West Conshohocken, PA, 2012.
[31] L. Fan, W. Meng, L. Teng, K.H. Khayat, Effect of steel fibers with galvanized coatings on corrosion of steel bars embedded in UHPC, Compos. B Eng. 177 (2019), 107445, https://doi.org/10.1016/j.compositesb.2019.107445.
[32] D. Gastaldi, F. Canonico, E. Boccaleri, Ettringite and calcium sulfoaluminate cement: investigation of water content by near-infrared spectroscopy, J. Mater. Sci. 44 (21) (2009) 5788–5794, https://doi.org/10.1007/s10853-009-3812-1.
[33] H. Kanada, Y. Ishikawa, T. Uomoto, Application of near-infrared spectroscopy for inspection concrete, Concr. J. 2 (3) (2005) 37–44, https://doi.org/10.3151/coj1975.43.3_37.
[34] K. Toda, Y. Nakamura, A. Kurata, System for diagnosing concrete deterioration with spectroscopic analysis, IHI Eng. Rev. 45 (1) (2012) 31–36, https://doi.org/10.3151/COJ1975.45.11_20.
[35] X. Wang, C. Shi, F. He, Q. Yuan, D. Wang, Y. Huang, Q. Li, Chloride binding and its effects on microstructure of cement-based materials, J. Chin. Ceram. Soc. 41 (2) (2013) 187–198, https://doi.org/10.7521/j.issn.0454%E2%80%935648.2013.02.11.